Supplemental Materials: Characterizing the Subglacial Environment of Lower Thwaites Glacier Using Radar Modeling

Chris PIERCE [1], Mark SKIDMORE [2,3], Lucas BEEM [2], Don BLANKENSHIP [4], Ed ADAMS [1], Christopher GEREKOS [4], Won Sang LEE [5]

[1] *Department of Civil Engineering, Montana State University, Bozeman Montana, USA*

[2] *Department of Earth Sciences, Montana State University, Bozeman Montana, USA*

[3] *Department of Physical Geography, Stockholm University, Stockholm, Sweden*

[4] *Institute for Geophysics, University of Texas at Austin, Austin Texas, USA*

[5] *Division of Glacial Environment Research, Korea Polar Research Institute, Seoul, South Korea*

Correspondence: Chris Pierce <christopherpierce3@montana.edu>

ABSTRACT. This document contains supplemental materials for *Characterizing the Subglacial Environment of Lower Thwaites Glacier Using Radar Modeling*. Supplements are as follows:

A - Homogeneous Fits

B - Hydrologic Fits

C - Substrate Transition Fits

D - Heterogeneous Fits

E - Simulation Methodology

SUPPLEMENTAL MATERIALS

A - Homogeneous fits

This section contains along-track relative reflectivity comparisons (R_{bed} vs. $R_{bed,S}$) and fit quality metrics for all simulated segments identified as homogeneous fits in the text. Simulation segment numbers correspond to locations on Fig. 2.

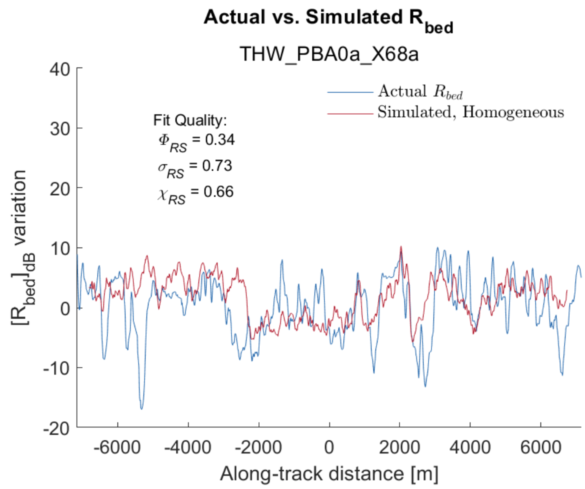

Fig. A1. Simulated segment 1, R_{bed} vs. $R_{bed,S}$ comparison

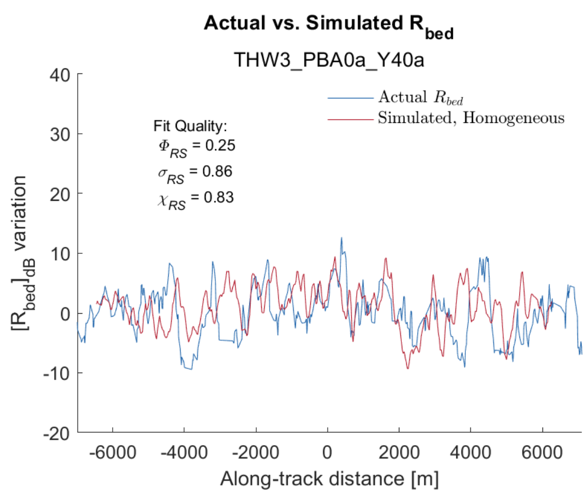

Fig. A2. Simulated segment 2, R_{bed} vs. $R_{bed,S}$ comparison

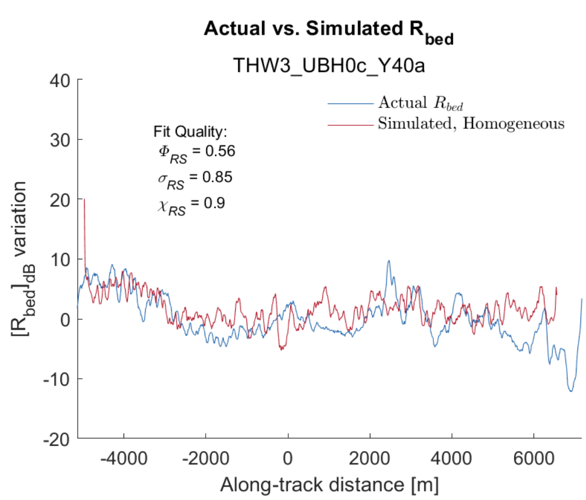

Fig. A3. Simulated segment 3, R_{bed} vs. $R_{bed,S}$ comparison

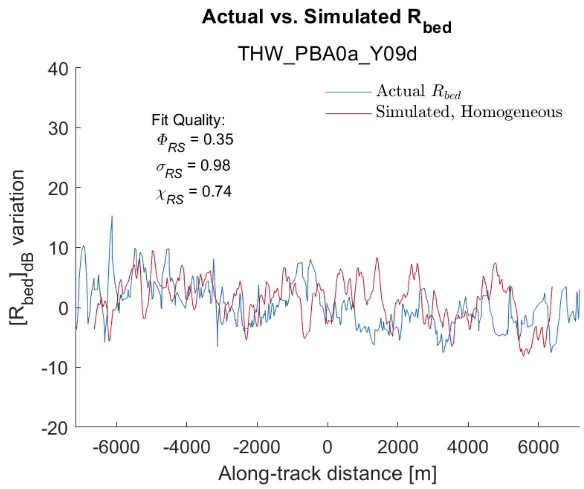

Fig. A4. Simulated segment 4, R_{bed} vs. $R_{bed,S}$ comparison

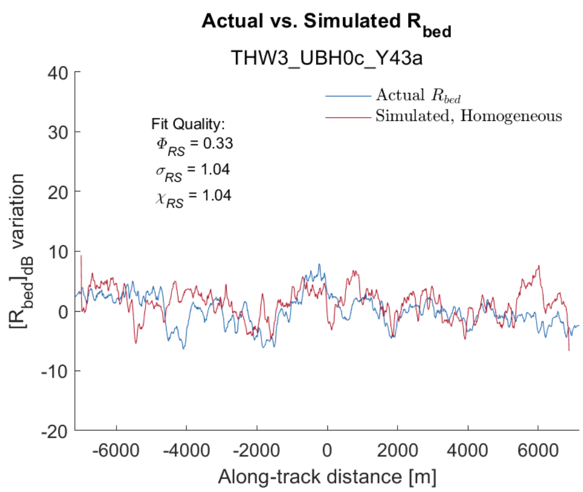

Fig. A5. Simulated segment 5, R_{bed} vs. $R_{bed,S}$ comparison

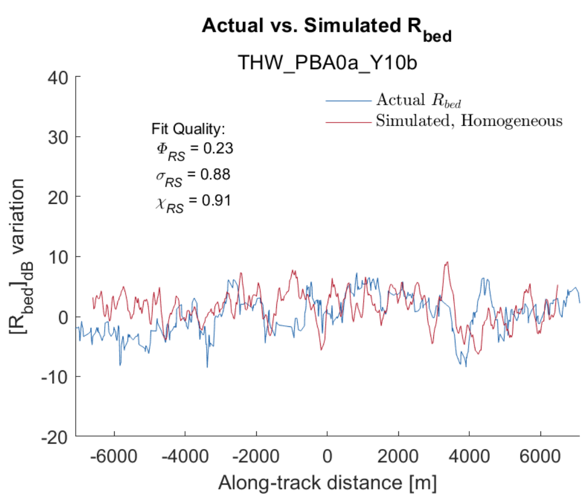

Fig. A6. Simulated segment 6, R_{bed} vs. $R_{bed,S}$ comparison

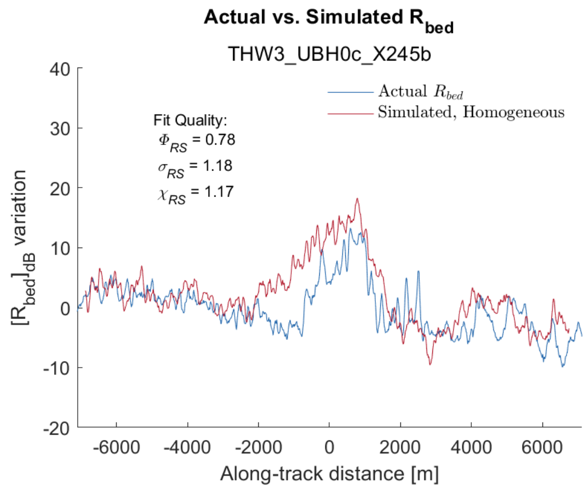

Fig. A7. Simulated segment 7, R_{bed} vs. $R_{bed,S}$ comparison

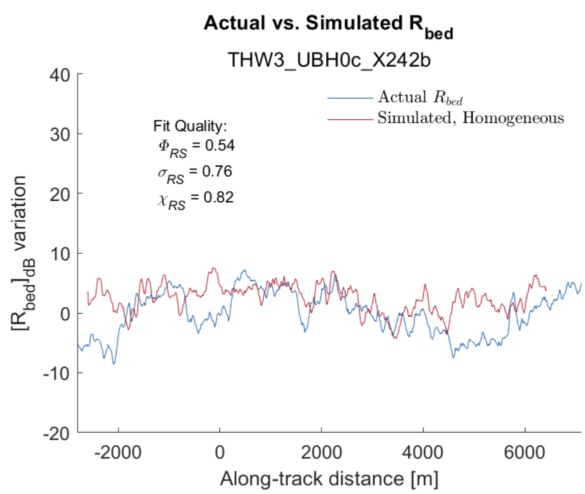

Fig. A8. Simulated segment 8, R_{bed} vs. $R_{bed,S}$ comparison

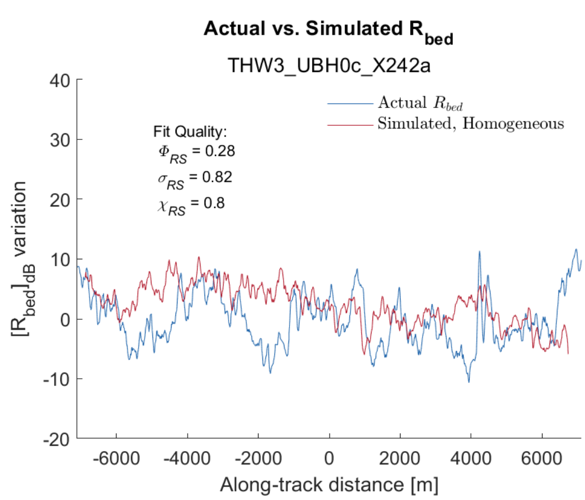

Fig. A9. Simulated segment 9, R_{bed} vs. $R_{bed,S}$ comparison

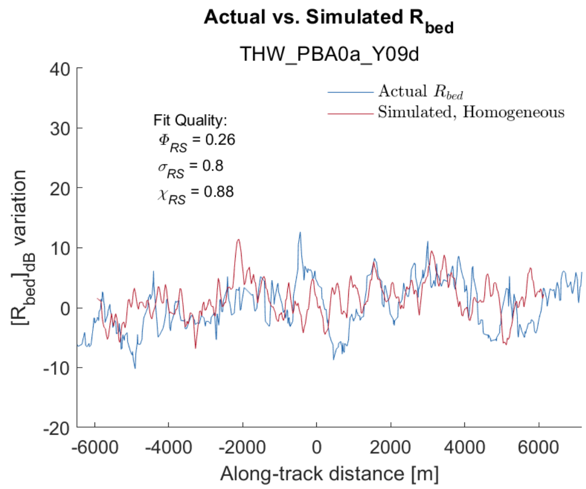

Fig. A10. Simulated segment 10, R_{bed} vs. $R_{bed,S}$ comparison

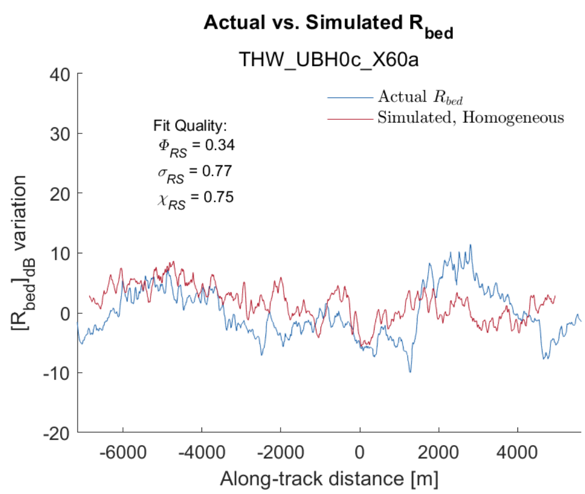

Fig. A11. Simulated segment 11, R_{bed} vs. $R_{bed,S}$ comparison

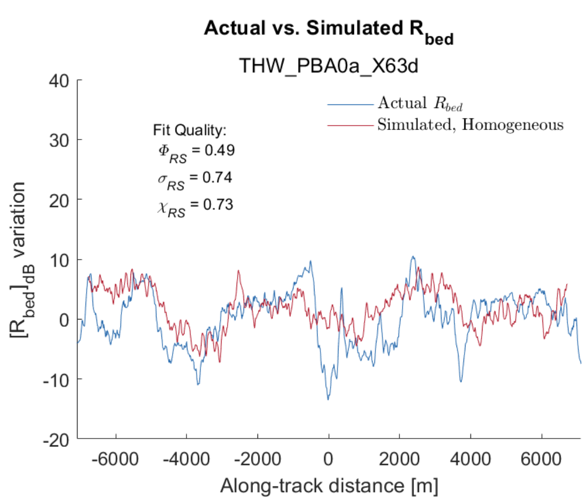

Fig. A12. Simulated segment 12, R_{bed} vs. $R_{bed,S}$ comparison

B - Hydrologic fits

This section contains along-track relative reflectivity comparisons (R_{bed} vs. $R_{bed,S}$) and fit quality metrics for all simulated segments identified as hydrologic fits in the text. For each graphic, panel a) shows the homogeneous simulation scenario, and b) shows the reflectivity comparison including regions with subglacial water. The grey shaded areas indicate where water was added to the simulation domain, with $\epsilon_{H_2O} = 78$ was simulated. Segment numbers correspond to locations on Fig. 2.

Note that for each simulation shown, water was added to a minimal number of locations in order to meet our established thresholds for fit quality. Therefore, these simulations may not necessarily represent a unique or optimal fit to the RES reflectivity if additional subglacial water was added to additional locations.

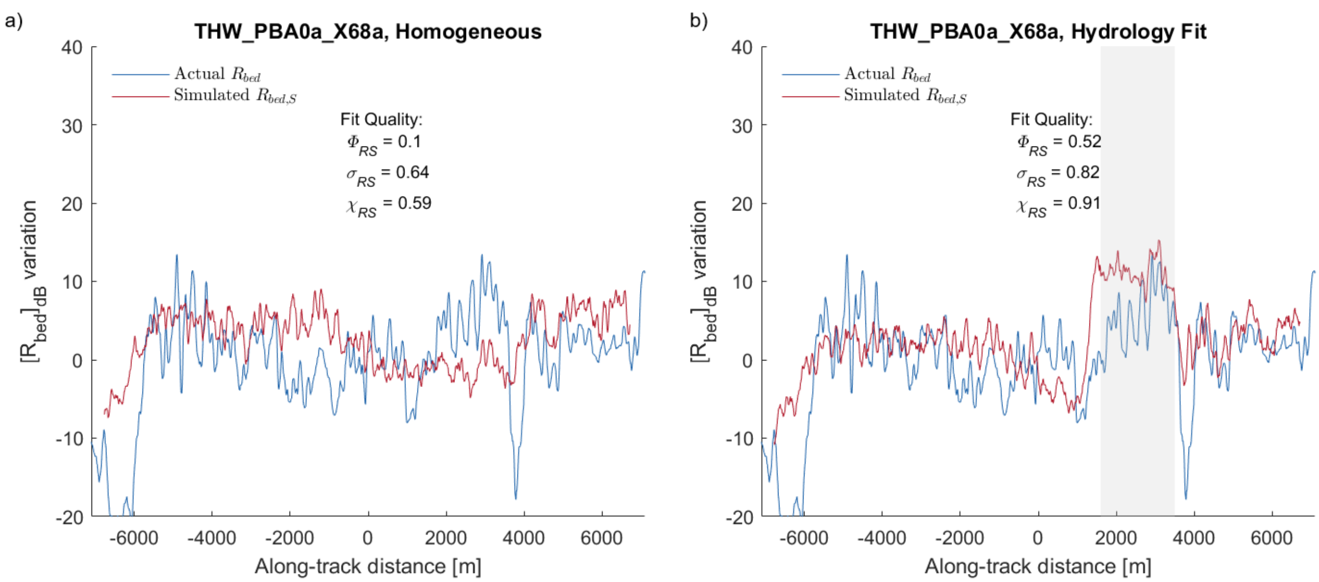

Fig. B1. Simulated segment 13, R_{bed} vs. $R_{bed,S}$ comparison

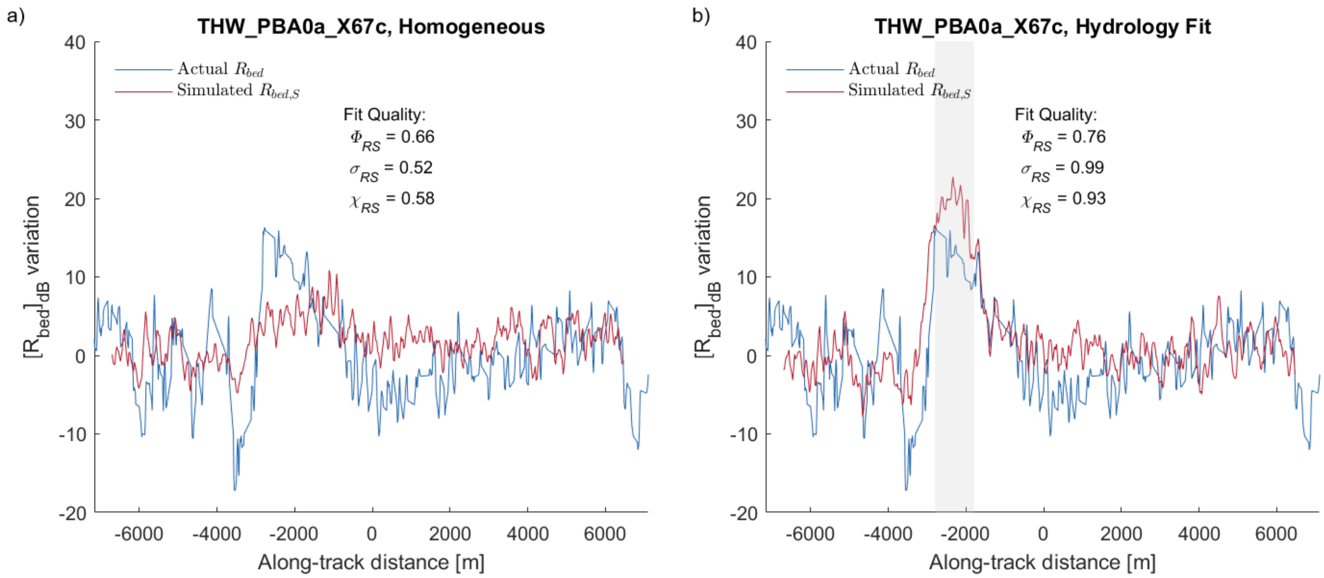

Fig. B2. Simulated segment 14, R_{bed} vs. $R_{bed,S}$ comparison

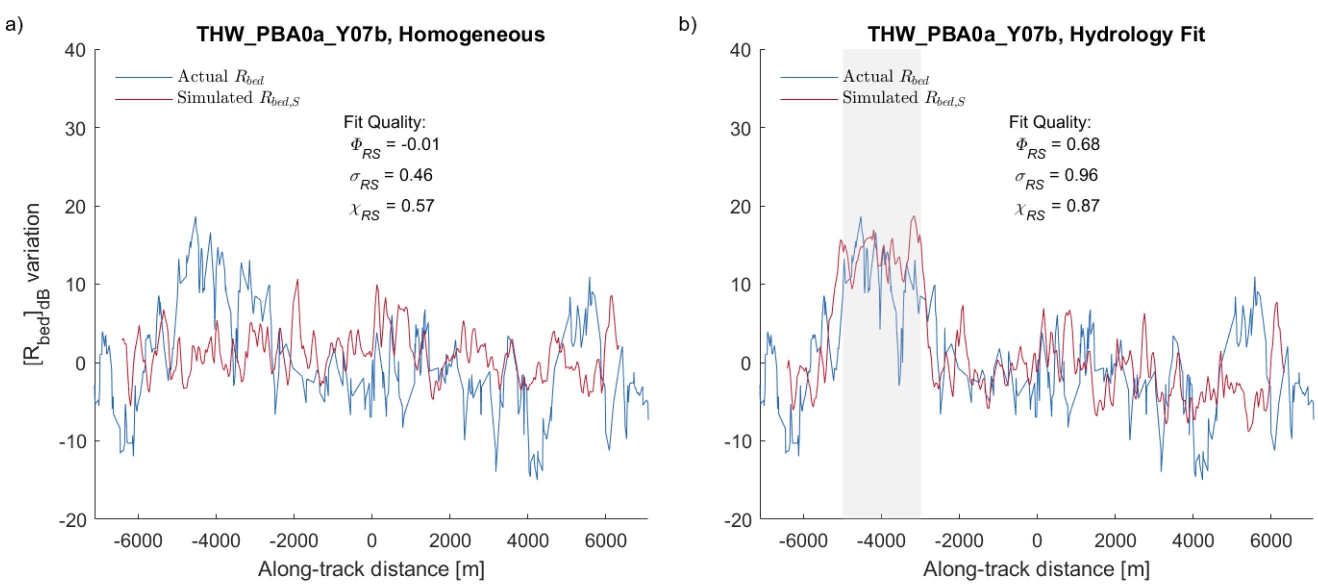

Fig. B3. Simulated segment 15, R_{bed} vs. $R_{bed,S}$ comparison

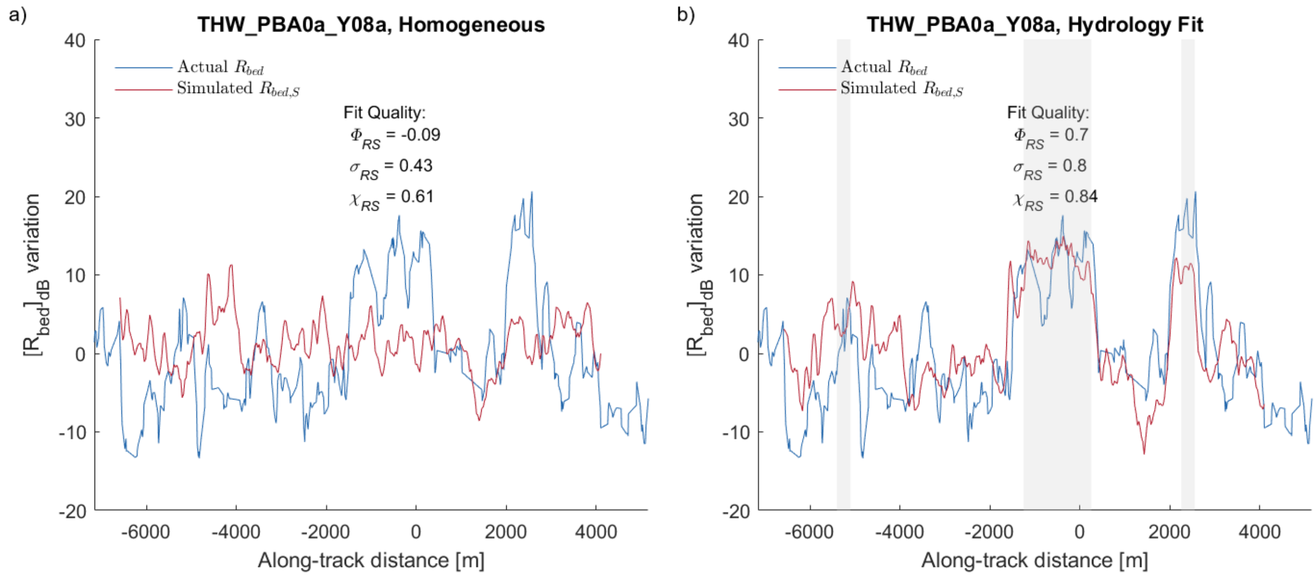

Fig. B4. Simulated segment 16, R_{bed} vs. $R_{bed,S}$ comparison

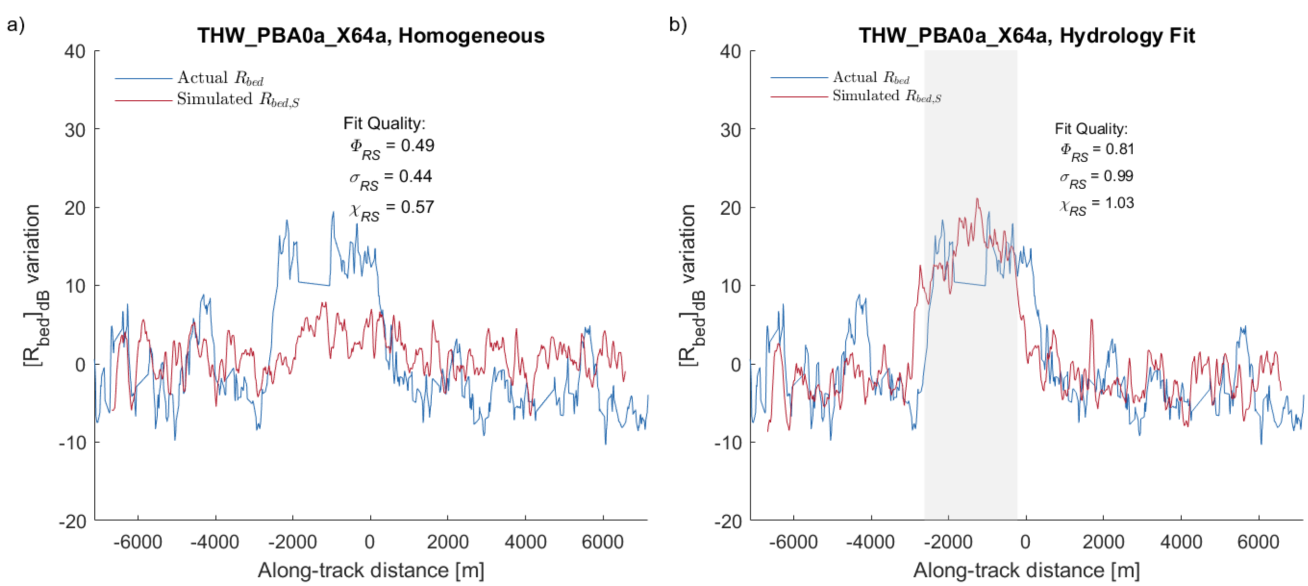

Fig. B5. Simulated segment 17, R_{bed} vs. $R_{bed,S}$ comparison

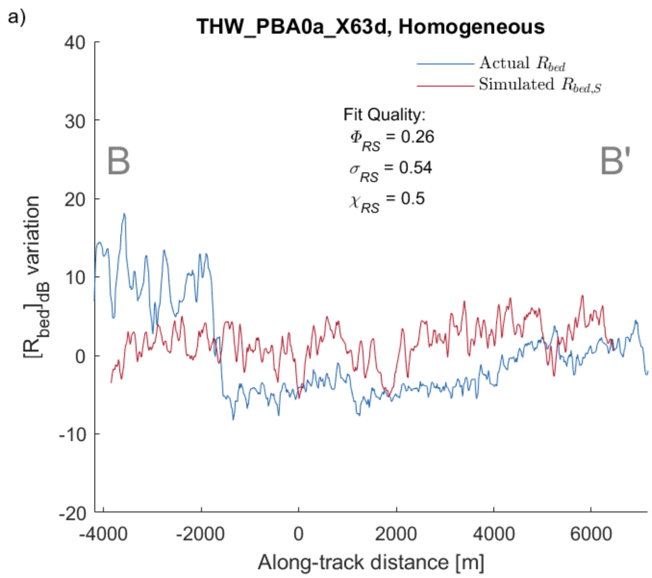

Fig. B6. Simulated segment 18, R_{bed} vs. $R_{bed,S}$ comparison

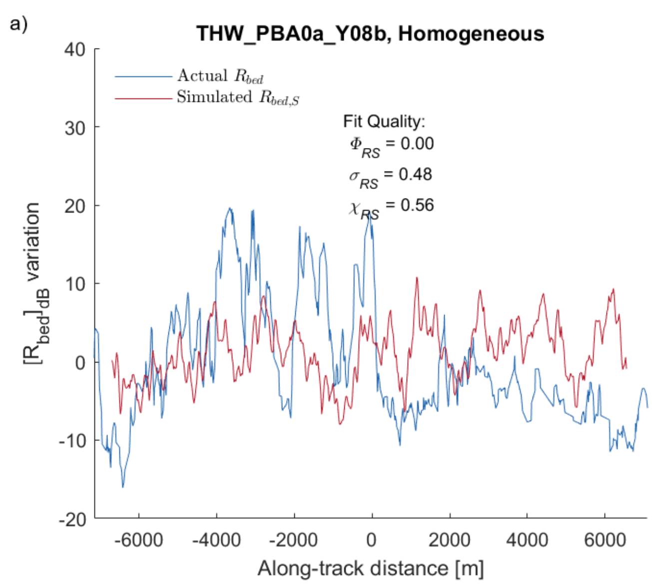

Fig. B7. Simulated segment 19, R_{bed} vs. $R_{bed,S}$ comparison

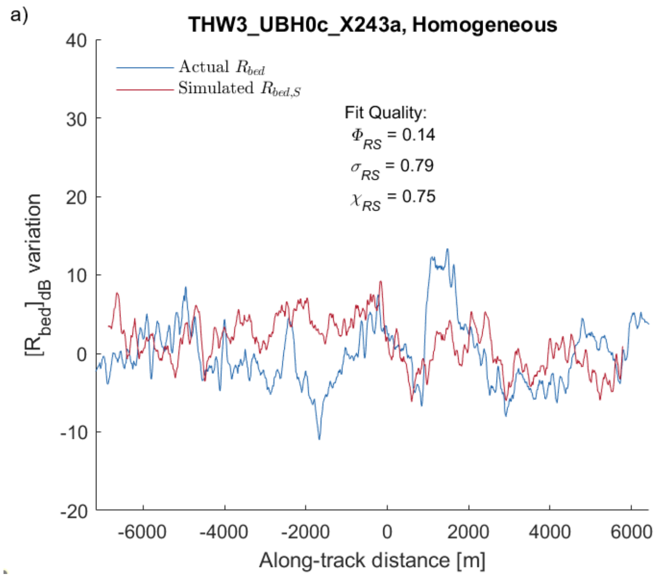

Fig. B8. Simulated segment 20, R_{bed} vs. $R_{bed,S}$ comparison

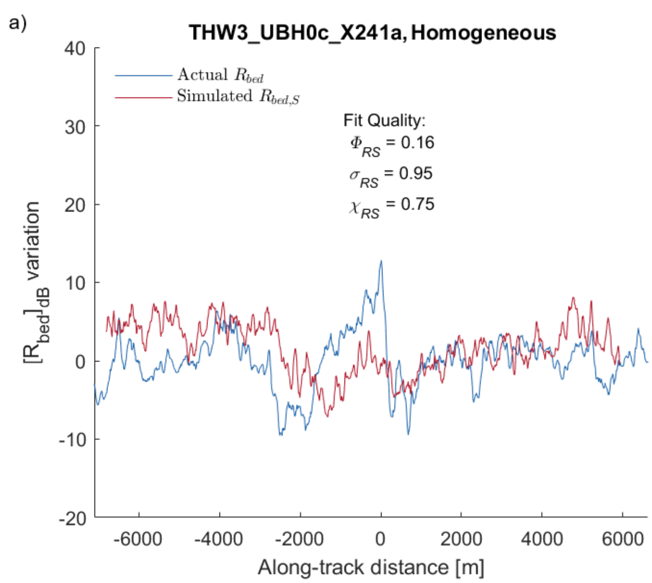

Fig. B9. Simulated segment 21, R_{bed} vs. $R_{bed,S}$ comparison

C - Substrate transition fits

This section compares along-track relative reflectivity (R_{bed} vs. $R_{bed,S}$) and fit quality metrics for all simulated segments identified as substrate transitions in the text. For each graphic, panel a) shows the homogeneous simulation scenario, and panel b) shows the reflectivity comparison with a substrate transition. The grey shaded area indicates locations where rough bedrock was simulated ($\sigma_{bed} = 1$ m, $\epsilon_{bed} = 5$), while the rest of the simulated bed has $\sigma_{bed} = 0.2$ m, $\epsilon_{bed} = 10$. Simulation segment numbers correspond to locations on Fig. 2.

Note that for each simulation shown, the substrate was altered at a minimal number of locations in order to meet our established thresholds for fit quality. Therefore, these simulations may not necessarily represent an optimal or unique fit to the RES reflectivity if other substrates were modeled in additional locations.

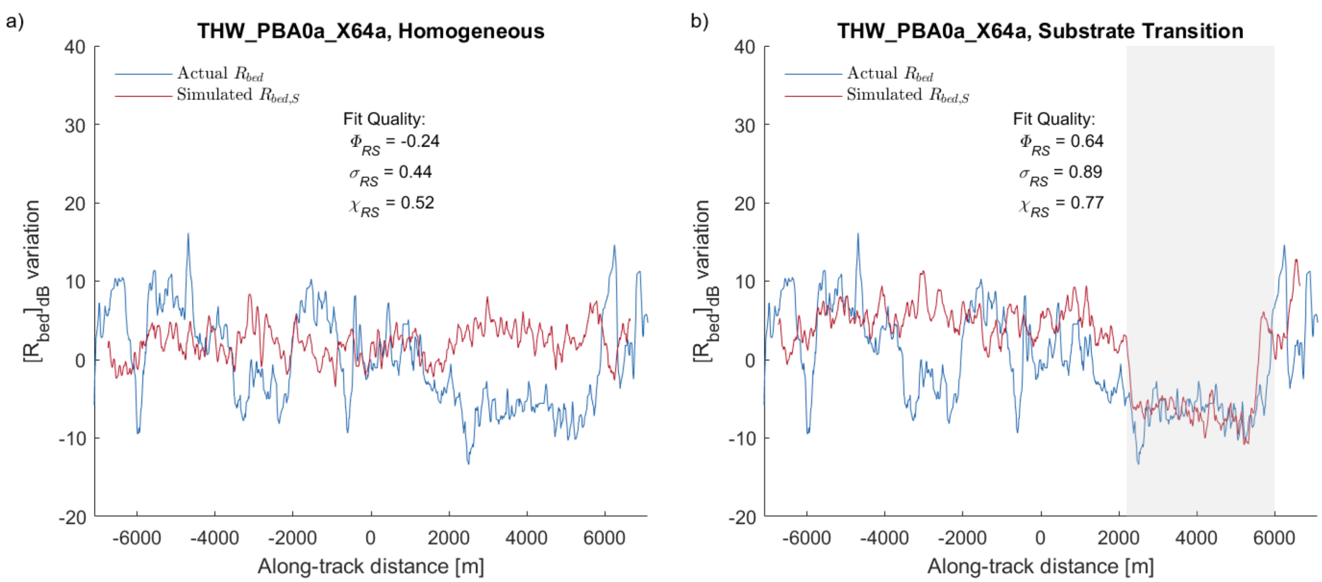

Fig. C1. Simulated segment 22, R_{bed} vs. $R_{bed,S}$ comparison

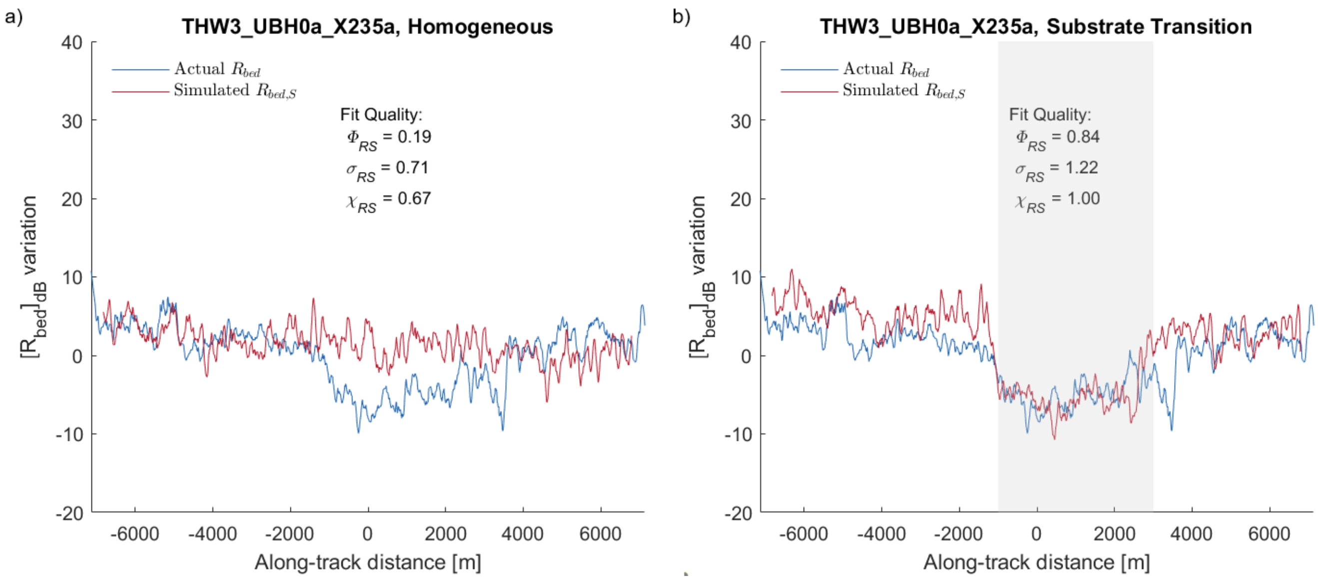

Fig. C2. Simulated segment 23, R_{bed} vs. $R_{bed,S}$ comparison

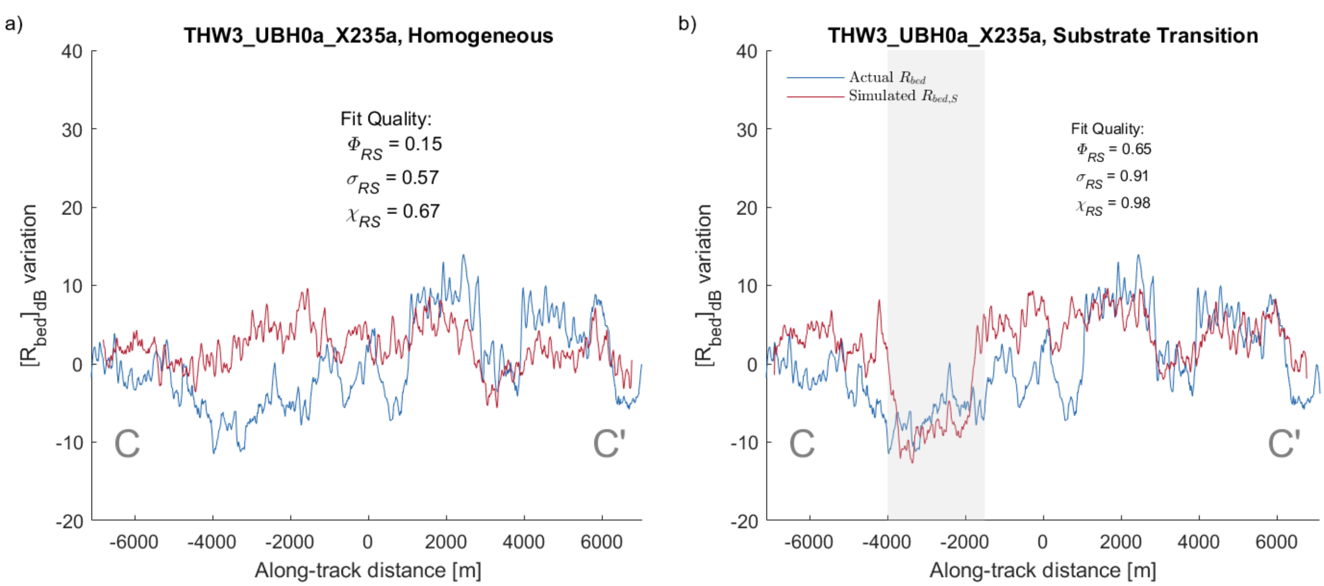

Fig. C3. Simulated segment 24, R_{bed} vs. $R_{bed,S}$ comparison

D - Heterogeneous fits

This appendix contains along-track relative reflectivity comparisons (R_{bed} vs. $R_{bed,S}$) and fit quality metrics for all simulated segments identified as heterogeneous in the text. Simulation segment numbers correspond to locations on Fig. 2.

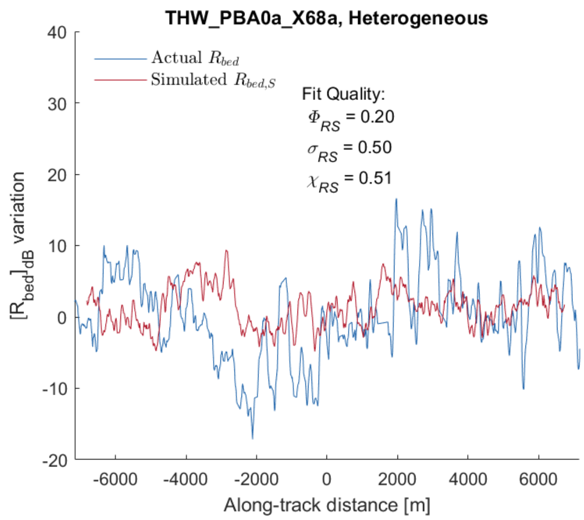

Fig. D1. Simulated segment 25, R_{bed} vs. $R_{bed,S}$ comparison

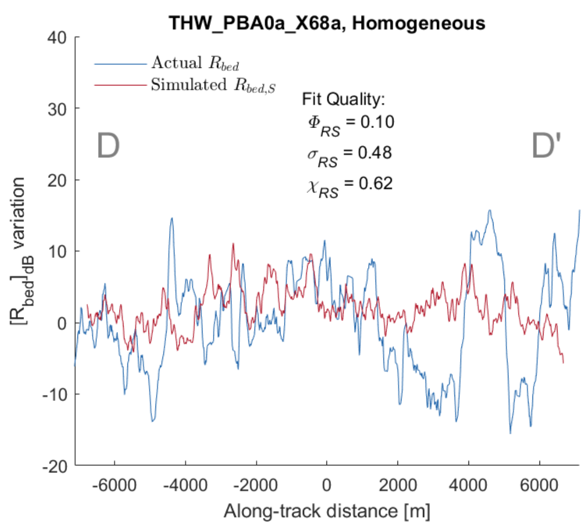

Fig. D2. Simulated segment 26, R_{bed} vs. $R_{bed,S}$ comparison

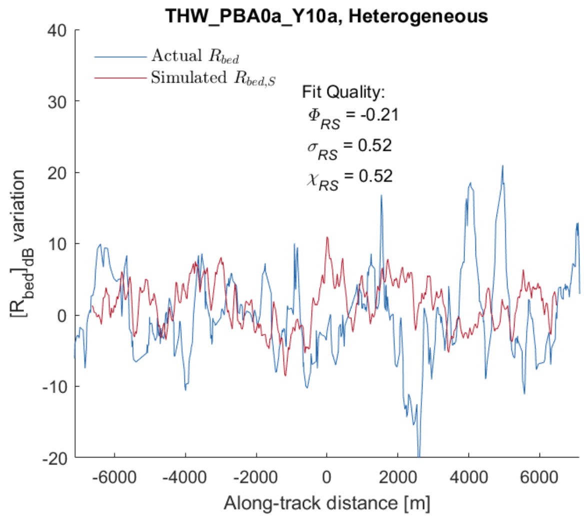

Fig. D3. Simulated segment 27, R_{bed} vs. $R_{bed,S}$ comparison

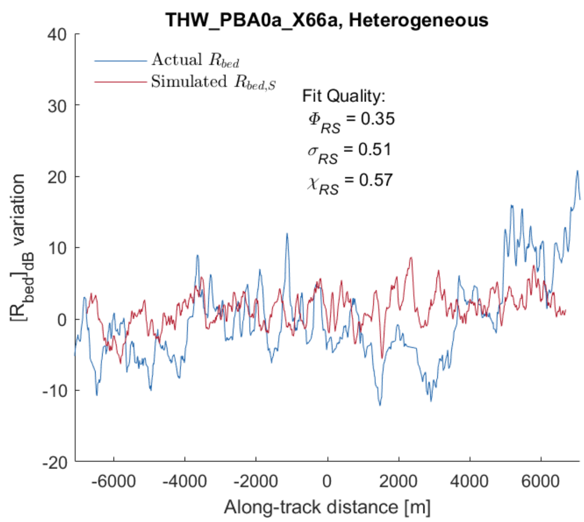

Fig. D4. Simulated segment 28, R_{bed} vs. $R_{bed,S}$ comparison

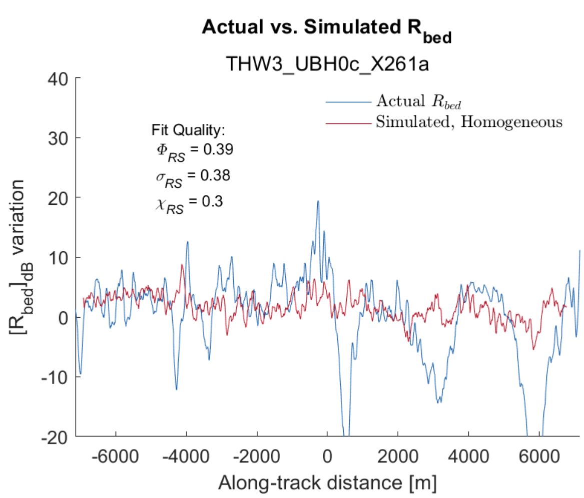

Fig. D5. Simulated segment 29, R_{bed} vs. $R_{bed,S}$ comparison

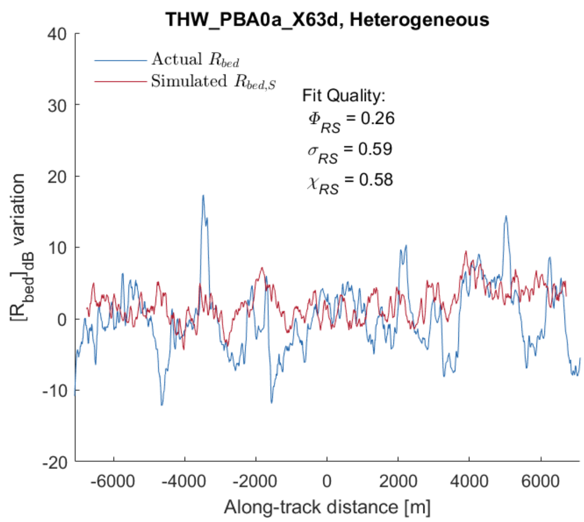

Fig. D6. Simulated segment 30, R_{bed} vs. $R_{bed,S}$ comparison

E - Simulation Methodology

The radar simulation method described in Pierce and others (2024) estimates variations in returned power vs. fast time by tracing the path and field strength of many individual rays transmitted through the ice surface then reflected from the bed. These data are compiled for a series of discrete locations y_i along a flight path to construct a simulated radargram. A conceptual model for the simulation process is depicted in Fig. E1.

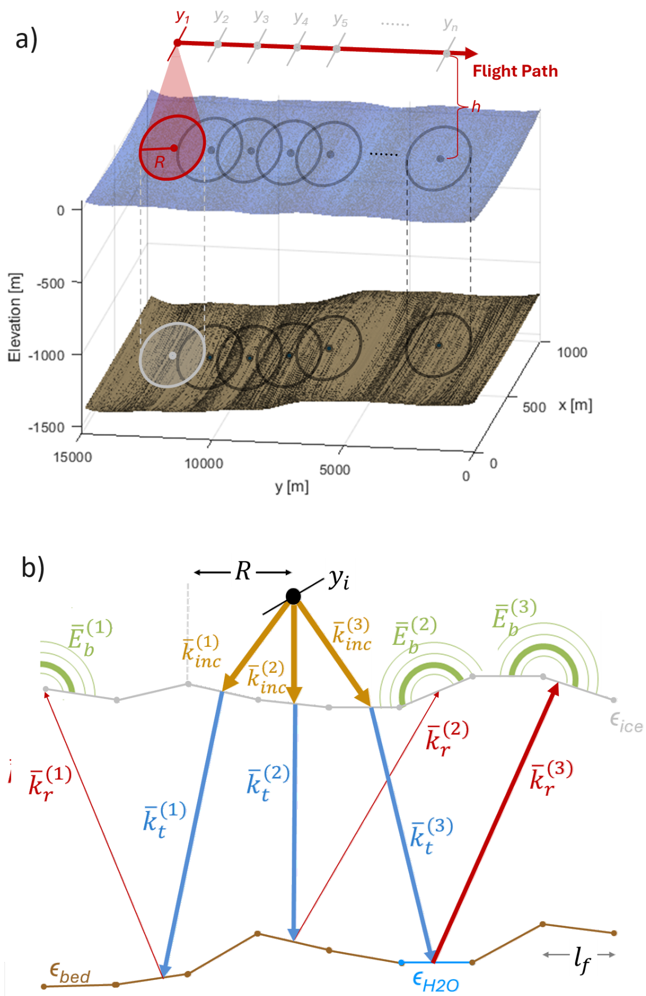

Fig. E1. Conceptual model of an RES simulation is depicted. a) Antenna position at height h is incremented in the y direction along a flight path above an ice and bed surface. b) A 2-D cross-section of the simulation is shown at a single position of the radar antenna in time and space, with location y_i. The radar directs an incident electromagnetic ray $\bar{k}_{inc}$ at each facet (length=l_f) within a footprint of radius R. The ray's direction and magnitude are traced through the ice and back to the surface, where the backscattered electric field $\bar{E}_b$ is estimated at the antenna. The relative magnitude of each ray is represented by the line thickness (not to scale).

The simulator requires Digital Elevation Models (DEM) for both the ice surface and glacier bed. These are derived from the actual RES surface and bed elevation data from the survey transect to be modeled.

Across-track topography is estimated with data from BedMachine V2 (Morlighem, 2020), creating a 3-dimensional environment for the simulation. Because across-track topography is estimated in this way, the simulation cannot accurately represent radar returns from unknown across-track topographic features (clutter).

Both DEMs are divided into facets with characteristic length l_f, and each facet is assigned a material dielectric constant ϵ. At the ice surface all facets are assigned ϵ_{ice}, while at the bed facets can be assigned a range of permittivity values based on location, presumed substrate materials, and hydrological structures being modeled. In order to maintain a relatively simple material model, we use $\epsilon_{H2O} = 78$ when modeling water structures, and $\epsilon_{sub} = 5 - 25$ for materials which could include hydrated bedrock, clays, or tills (Peters and others, 2005; Christianson and others, 2014; Tulaczyk and Foley, 2020). By default, we assume $\epsilon_{sub} = 5$ to represent bedrock in our material model unless otherwise noted.

Simulated radar attenuation in ice is controlled through the imaginary component of ϵ_{ice}. This value, otherwise known as the loss tangent ($\tan\delta$), is related to attenuation rate via Eq. E1, where λ is the radar wavelength and η_{ice} is the square root of the real component of ice permittivity (Peters and others, 2005).

$$\langle N_{ice} \rangle = \frac{20\pi\eta_{ice}\log_{10} e}{\lambda} \tan\delta \tag{E1}$$

A flight path is defined at a height above the ice surface h. We choose a simulation radius R, which bounds the simulation scope at each position along the simulated flight path for efficiency. R for all simulations was between 300-350 m, chosen primarily to facilitate sufficient range migration during Synthetic Aperture Radar (SAR) focusing as described in Pierce and others (2024). We note that this bound on R means the simulation will not include clutter from across-track features competing with the subsurface feature, which is a potential limitation of the method. All other relevant simulation parameters listed in Table E1 are intended to emulate a helicopter-based MARFA experiment.

The individual simulated observations of returned power vs. fast time (τ) are compiled along the y axis. This forms a simulated raw radargram, which estimates the returned power from the topographic and material model. Further radargram processing is consistent with real RES processing. The radargram is range compressed and focused in azimuth (Pierce and others, 2024), although the focusing aperture length is shorter due to computational constraints. Simulated bed reflectivity $R_{bed,S}$ is then defined at the sample with maximum returned power between user defined bounds in the radargram.

Table E1. Summary of parameters used in RES simulations of Thwaites Glacier.

Parameter	**MARFA Value**
Aircraft height (h)	$500\,m$
Aircraft velocity (v_a)	$30\ ms^{-1}$
Facet length (l_f)	$5\ m$
Simulation Radius (R)	$300 - 350\,m$
Correlation length (l_c)	$15\,m$
Surface roughness (σ_{ice})	$0.2\,m$
Basal roughness (σ_{bed})	$0.2 - 1\,m$
Center frequency (f_c)	60 MHz
Bandwidth (B_w)	15 MHz
PRF[a]	6400 Hz *(30 Hz)*
Sampling frequency (f_s)	50 MHz
Pulse length (T_s)	$1\ \mu s$
Receiving window (T_r)	$50\ \mu s$
Ice Permittivity (ϵ_{ice})	$3.18\,(1 + .0015i)$[b]
Substrate Permittivity (ϵ_{sub})	$5 - 25$
Water Permittivity (ϵ_{H_2O})	78

[a]Native PRF for MARFA radar is 6400 Hz. Simulations are run at 30 Hz to replicate effective PRF after coherent summation during data processing.

[b]Ice $\tan\delta = 0.0015$ was chosen to simulate the average estimated attenuation from the RES surveys, $\langle N_{ice} \rangle = 14.35$ dB km^{-1}

REFERENCES

Christianson K, Peters LE, Alley RB, Anandakrishnan S, Jacobel RW, Riverman KL, Muto A and Keisling BA (2014) Dilatant till facilitates ice-stream flow in northeast Greenland. *Earth and Planetary Science Letters*, **401**, 57–69, ISSN 0012-821X (doi: 10.1016/J.EPSL.2014.05.060)

Morlighem M (2020) MEaSUREs BedMachine Antarctica, Version 2 (doi: 10.5067/E1QL9HFQ7A8M)

Peters ME, Blankenship DD and Morse DL (2005) Analysis techniques for coherent airborne radar sounding: Application to West Antarctic ice streams. *Journal of Geophysical Research: Solid Earth*, **110**(6), 1–17, ISSN 21699356 (doi: 10.1029/2004JB003222)

Pierce C, Gerekos C, Skidmore M, Beem L, Blankenship D, Lee WS, Adams E, Lee CK and Stutz J (2024) Characterizing sub-glacial hydrology using radar simulations. *The Cryosphere*, **18**(4), 1495–1515 (doi: 10.5194/tc-18-1495-2024)

Tulaczyk SM and Foley NT (2020) The role of electrical conductivity in radar wave reflection from glacier beds. *The Cryosphere*, **14**(12), 4495–4506, ISSN 19940424 (doi: 10.5194/tc-14-4495-2020)